Macromolecular Bioscience
www.mbs-journal.de

Hemocompatible and Bioactive Heparin-Loaded PCL-α-TCP Fibrous Membranes for Bone Tissue Engineering

Morteza Alehosseini, Nasim Golafshan, Mahshid Kharaziha, Mohammadhossein Fathi, and Hossein Edris*

The combination of bioactive components such as calcium phosphates and fibrous structures are encouraging niche-mimetic keys for restoring bone defects. However, the importance of hemocompatibility of the membranes is widely ignored. Heparin-loaded nanocomposite poly(ε-caprolactone) (PCL)-α-tricalcium phosphate (α-TCP) fibrous membranes are developed to provide bioactive and hemocompatible constructs for bone tissue engineering. Nanocomposite membranes are optimized based on bioactivity, mechanical properties, and cell interaction. Consequently, various concentrations of heparin molecules are loaded within nanocomposite fibrous membranes. In vitro heparin release profiles reveal a sustained release of heparin over the period of 14 days without an initial burst. Moreover, heparin encapsulation enhances mesenchymal stem cell (MSC) attachment and proliferation, depending on the heparin content. It is concluded that the incorporation of heparin within TCP–PCL fibrous membranes provides the most effective cellular interactions through synergistic physical and chemical cues.

1. Introduction

Recently, thanks to the similarity of the chemistry and architecture with the surrounding host tissue, autogenic bone graft implantation has been demonstrated as the clinical gold standard for bone defects arising from diverse diseases, osteosarcoma, and traumas.[1,2] Nonetheless, the inadequate accessibility and donor site injury associated with autografts confine their widely application in the clinic approaches.[3] Therefore, there is significant interest in developing of alternatives consisting of allografts, xenografts and tissue engineering approaches.[4] Bone tissue engineering aims at refining the strength of musculoskeletal tissue via incorporation of a bone graft substitute to encourage formation of bone from the surrounding tissue or to act as a template for inserted bone cells.[4] There are several strategies suggested by tissue engineering to regenerate bone tissue which do not need secondary surgery such as bone cement to fill cavity,[4] and bone scaffolds[5] and membranes.[6,7] Between them, the membranes could provide the appropriate environment for new tissue growth without stimulation immune system responses.[8] In order to accelerate functional cell progressions which are crucial for tissue regeneration, porous membranes need to morphologically, chemically and physically mimic the host tissue.[9–11] In this way, numerous studies have focused on fibrous biodegradable membranes for bone tissue engineering applications. Several biodegradable polymers such as poly(L-lactic acid) (PLA),[12] poly (lactic-*co*-glycolic acid) (PLGA),[13] and poly(caprolactone) (PCL)[14] have been widely used for bone tissue engineering applications. Between them, PCL is a synthetic and biodegradable polymers with slow degradation rate, ability to protect defect site for complete healing, good biocompatibility, and high drug permeability which are suitable for use in long term load bearing applications.[15] Despite its significant characteristics, the shortcomings such as low mechanical properties, poor osteogenic properties, and bone regeneration capacity restrict widespread applications of pure PCL. Therefore, nanocomposite membranes based on PCL combined with bioactive components were developed to reproduce the osteogenic niches offered by autografts. Recently, bioactive components consisting of hydroxyapatite (HA),[16] tricalcium phosphate (TCP),[4,14,17,18] forsterite,[8] diopside,[19] and biphasic calcium phosphate (BCP)[20] have been applied to reproduce the osteogenic niche offered by autografts. Among these ceramics, Ca–P based ceramics such as TCP ($Ca_3(PO_4)_2$) has drawn an excessive deal of attention for bone tissue engineering applications owing to its biocompatibility, osteoconductivity, and resobability.[21,22] TCP-based ceramics reveal higher resorption rate than HA, and have ability to hydrate and set into calcium deficient hydroxyapatite (CDHA, $Ca_{10-x}(HPO)_x(PO_4)_{6-x}(OH)_{2-x}$, x = 0–1) at near physiological pH and temperature.[23–25] TCP has two main polymorphous which are stable at high and low temperatures known as α-TCP and β-TCP, respectively. Owning to superior osteoconductivity of α-TCP compared to β-TCP, α-TCP ceramic has been widely applied as a bioactive component for bone tissue engineering. α-TCP also shows higher resorbability and activity than β-TCP which provides phosphate and calcium ions by hydrolysis which promotes bone formation.[26,27] Although wide investigations have focused on the nanocomposite scaffolds based on polymers and calcium phosphates for bone tissue engineering,[28] limited researches applied α-TCP particles in polymeric matrix.

M. Alehosseini, N. Golafshan, Dr. M. Kharaziha, Prof. M. H. Fathi, Prof. H. Edris
Department of Materials Engineering
Isfahan University of Technology
Isfahan 84156-83111, Iran
E-mail: kharaziha@cc.iut.ac.ir

DOI: 10.1002/mabi.201800020

For instance, Bennett et al.[29] developed resorbable composites based on poly(D,L-lactide-*co*-glycolide) (PLGA) reinforced with nano- and micro-particles of α-TCP. Results showed that the incorporation of α-TCP nanopowder modulated the degradation rate and enhanced the biological and mechanical properties. In another research, composite polymeric matrix of polymethylmethacrylate (PMMA) and α-TCP was fabricated to evaluate the biological properties for bone repair. The results showed that PMMA+α-TCP significantly affected osteoblast viability.[30] These findings pointed out the potential use of α-TCP in controlling composite osteodonductivity whilst maintaining good bone formation.

When the synthetic membranes interfere with living tissues or blood, surface-induced thrombosis happens at the blood–biomaterial interface. Therefore, synthetic membranes with blood compatible surfaces have attracted great interest in tissue engineering applications.[31] Various strategies have been applied to develop antithrombotic and hemocompatible constructs consisting of surface heparinization,[32] heparin-functionalized polymers,[33] and heparin encapsulation in the polymer matrix.[34] Between these approaches, owing to the accurately controlled release of the incorporated drug over periods of hours to months, encapsulation of blood compatible drugs such as heparin within biodegradable membranes could be more promising approach. Heparin is a linear glycosaminoglycan consisting of sulfated repeating disaccharide unit, which has been recognized as a biologically important biomolecule.[35] Heparin has been widely applied in various scaffolds and membranes to improve their hemocompatibility.[31,36] For instance, the electrospun silk fibrin membrane were grafted by heparin and resulted in promoted proliferation of fibroblasts.[37] More recently, in addition to improved hemocompatibility, results showed that heparin could affect the functions of osteoblast cells, such as osteoblast-like MC3T3-E1.[38,39] For instance, Cao et al. studied on the GBR membrane based on PCL containing basic fibroblast growth factor and heparin.[40] They showed that heparin-PCL membrane exhibited larger projected areas than PCL one which was appropriate for osteoblast like cells to attach, proliferate, and differentiate. To the best of the present authors' knowledge, limited studies have been performed on the release of heparin from bioactive membranes. It is expected that dual therapy approach via incorporation of an anti-thrompogenic drug into a bioactive and biodegradable membranes could provide a crucial purpose in biomedical applications. These membranes may inhibit blood coagulation while fills the bone defect supporting local tissue regeneration.

Herein, we report development and in vitro evaluation of bioactive, biocompatible and hemocompatible fibrous membrane of PCL-α-TCP for filling bone defects. Due to the complexity of synthesis α-TCP nanopowder,[41,42] there is no research in which α-TCP nanopowder as a superior osteoconductive particle incorporated in PCL fibers to enhance the bone regeneration and mechanical properties. So, by incorporation of Si into the TCP structure, α-TCP nanopowder was stabilized at lower temperature and could be used as superior osteoconductive particles in bone tissue engineering. After optimization of the α-TCP content based on mechanical, structural, chemical, and biological properties of PCL-α-TCP fibrous membrane, the amount of encapsulated heparin on the hemocompatibility and cellular behavior of the heparin incorporated PCL-α-TCP fibrous scaffold was investigated. Moreover, heparin release mechanism from PCL-α-TCP fibrous membrane was investigated. It is hypothesized that the development of a hemocompatible, bioactive, and robust fibrous membrane could simultaneously induce proper cues to support bone cell functions.

2. Experimental Section

2.1. Materials

PCL (M_w = 80 000 gr/mol) and heparin sodium salt from porcine intestinal mucosa were purchased from Sigma-Aldrich, Germany. Chloroform, methanol, ethanol, calcium nitrate tetrahydrate ($Ca(NO_3)_2 \cdot 4H_2O$), phosphorus pentaoxide (P_2O_5), and amorphous silica (SiO_2) were provided from Merck, Germany. Phosphate buffered saline (PBS), Dulbecco's modified Eagle's medium (DMEM-low), fetal bovine serum (FBS), and penicilin/streptomycin were prepared from Bioidea, Iran. 3-(4,5-dimethylthiazol-2-yl)-2,5- diphenyl tetrazolium (MTT) and dimethyl sulfoxide (DMSO) were purchased from Sigma, USA.

2.2. Synthesize and Characterization of Si-Stabilized α-TCP Nanopowder

Si-stabilized α-TCP powder was synthesized in a two-step process of sol–gel and mechanical alloying, according to the recent research.[4] **Figure 1** schematically presents Si-stabilized α-TCP synthesize process. Primarily, CDHA was synthesized using P_2O_5 (1 M) and $Ca(NO_3)_2 \cdot 4H_2O$ (3 M) in ethanol with Ca/P molar ratio of 1.5. After mixing two solutions and stirring for 1 day, the final solution was aged for 24 h at room temperature and consequently dried at 110 °C for 24 h. Finally, CDHA was synthesized using calcification at 600 °C for 1 h. In order to synthesize Si-stabilized α-TCP, as-prepared CDHA was mixed with amorphous silica in weight ratio of $SiO_2/(CDHA + SiO_2) = 1.88$, corresponded to 0.89 wt% Si. After 20 min sonication in 30 mL double distilled water (DDW) to improve the homogeneity of the mixture, the final slurry was milled in a planetary ball mill (Restsch PM100, Germany) using four agate balls (diameter 15 mm) at 250 rpm for 10 h. The mixture was dried for 24 h at 110 °C and finally was calcified at 1250 °C for 2 h. The heating rate was set at 5 °C min^{-1} and the samples were cooled in furnace.

X-ray powder diffraction (XRD, X'Pert Pro X-ray diffractometer, Phillips, Netherlands) was performed with Cu Kα radiation (λ = 0.154 nm, 40 kV, 40 mA) to characterize the phase composition of Si-stabilized α-TCP. Furthermore, to investigate the chemical composition of the Si-stabilized α-TCP nanopowder, Fourier transform infrared spectroscopy (FTIR, Bruker tensor) was performed over a range of 400–1400 cm^{-1} and resolution of 2 cm^{-1}. The morphology and particle size of Si-stabilized α-TCP powders were also investigated using transmission electron microscope (TEM, Philips EM208S 100 kV, Netherland). In this regard, the dispersed powders in water were sonicated for 10 min and, finally, were deposited on a carbon grate.

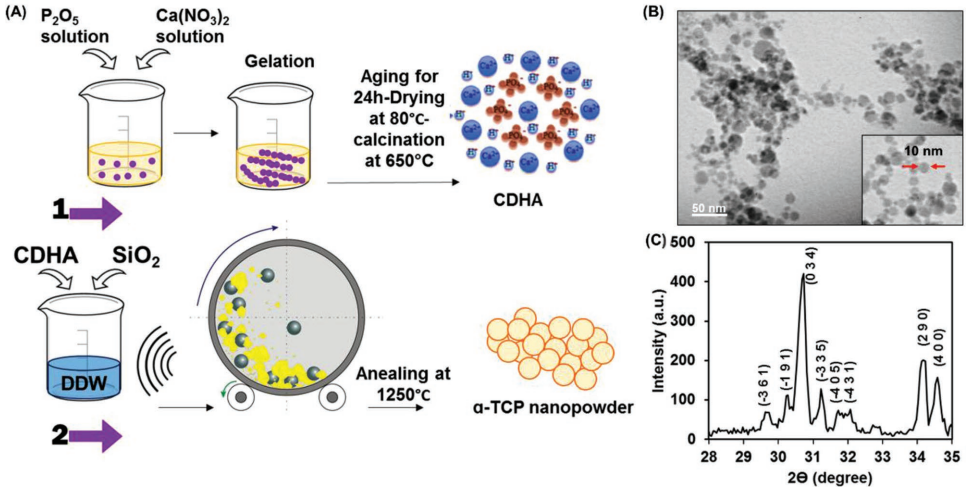

Figure 1. A) Schematic diagram describing the synthesize process of α-TCP nanopowders consisting of two steps: preparation of CDHA nanoparticles (step 1) and mixing CDHA with SiO_2 using ball milling. B) TEM image and C) X-ray diffraction pattern of α-TCP nanopowder after annealing at 1250 °C.

2.3. Development of α-TCP-PCL and Heparin-Loaded PCL-α-TCP Fibrous Membranes

Nanocomposite fibrous membranes with various concentrations of Si-stabilized α-TCP were developed using electrospinning technique. After preparation of 10 wt% PCL solution in chloroform:methanol (8:2 v/v), Si-stabilized α-TCP powder was added in order to provide various concentrations of Si-stabilized α-TCP nanopowder within PCL solution (0, 0.5, 1, and 2 wt%). After 30 min sonication, the suspensions were fed into 1 mL syringe having a 23G blunted stainless steel needle. Electrospinning was performed while working parameters consisting of flow rate (0.5 mL h^{-1}), the distance between the collector and the needle (15 cm) and voltage (20 kV) were kept constant. The nanocomposite membrane, collected on the aluminum foil, was dried overnight under vacuum prior to further characterizations. According to amounts of Si-stabilized α-TCP content (0.5, 1, and 2 wt%), samples were named PCL-0.5α, PCL-1α, and PCL-2α, respectively.

In order to develop heparin-loaded PCL-α-TCP fibrous membranes, desired amount of heparin was dissolved in 20 µL water and mixed with ≈400 µL methanol. Consequently, various amounts of heparin solution were added to PCL-α-TCP solutions with optimized concentration of Si-stabilized α-TCP (PCL-1α sample) to prepare heparin-loaded PCL-α-TCP membrane with 0.1, 1, and 2 wt% heparin. According to amount of loaded heparin (0.1, 1, and 2 wt%), the membranes were labeled with (PCL-1α)-0.1hep, (PCL-1α)-1hep, and (PCL-1α)-2hep, respectively. Consequently, the suspensions were transferred to a 1 mL syringe attached to a blunt end metal capillary with a 0.5 mm internal diameter. Finally, electrospinning process was selected at a flow rate of 0.5 mL h^{-1} and voltage of 20 kV (15 cm).

2.4. Characterizations of Fibrous Membrane

The morphology of the fibrous membranes was investigated using scanning electron microscope (SEM, Philips, XL30). Before imaging, the samples were sputter coated with a thin layer of gold. The fiber and pore size of the electrospun fibrous membrane was also determined (n = 30) using SEM images along with NIH ImageJ software. Attenuated total reflectance FTIR spectroscopy (ATR-FTIR, Bruker tensor) in the range of 400–4000 cm^{-1} was applied before and after heparin loading in order to evaluate chemical composition of the membranes.

Mechanical properties of PCL-α-TCP fibrous membrane fibrous membrane were also determined using a tensile tester (Hounsfield H25KS) with a load cell capacity of 10 N at 2 mm min^{-1} rate with dimension of 10 × 40 mm^2 and average thickness of 200 µm (n = 5). After plotting the stress-strain curves, the mechanical properties consisting of energy per volume (toughness), strain at break (elongation), tensile strength, and modulus (0–4% strain) were calculated.

To investigate the bioactivity, the fibrous membranes with size of 10 mm × 10 mm (n = 3) were immersed in simulated body fluid (SBF) solution. After 28 days, the membrane washed with DDW and, consequently, dried in air at room temperature. The apatite formation ability of the membranes was examined using scanning electron microscopy and EDX (SEM, Philips, XL30) and XRD (X'Pert Pro X-ray diffractometer, Phillips, Netherlands). In vitro degradation assay was applied to determine weight loss of the fibrous membranes. Three samples of each type of different membranes with weight of about 35 mg were incubated in PBS at 37 °C for 7, 14, 21, and 28 days, where the pH was near identical to the physiological conditions (pH = 7.4). PBS was refreshed every 3 days. At time point, the samples were rinsed with PBS, dried and weighted. Finally, the degradation percentage was estimated via dividing the weight loss by the initial dry weight. Also, the swelling behavior of fibrous membranes was assessed in PBS for a period of 24 h at 37 °C and pH = 7.4 according to previous research.[43] The hydrophilicity of the PCL-α-TCP fibrous membranes (n = 5) was evaluated using water contact angle measurement with a Drop Shape Analysis System (Sessile Drop, G10). 4 µL water droplet was applied in the measurements and the contact angle between the drop and the membranes was estimated at the first second of falling drop on them.

2.5. Heparin Release Study

Sterilized heparin-loaded PCL-α-TCP fibrous membranes were placed in 2 mL of pre-warmed PBS and incubated at 37 °C over a 14 day period. At each time point (1 h, 3 h, 6 h, 24 h, 72 h, 5 days, 8 days, and 12 days), 100 µL of PBS consisting of released heparin was discarded and replaced with fresh PBS. Finally, released heparin was quantified from fluorescence intensity of the release media at 490 nm. In order to evaluate the amount of heparin at specific time points, heparin standard curve was drawn by using the specific concentration of heparin (50, 10^2, 10^3, 10^4, 10^5, and 10^6 ng mL^{-1}) in PBS versus optical density of samples in 490 nm. The effects of various concentrations of loaded heparin on the release kinetic were studied according to Equations (1) and (2)[6]

$$\frac{\mathrm{M}}{M_t} = kt^n \tag{1}$$

$$\frac{M}{M_t} = \left(\frac{16 D_{\mathrm{app}} t}{\pi H^2}\right)^{0.5} \tag{2}$$

in which k and n are the rate parameter and diffusional exponent, respectively. Furthermore, D_{app} is the apparent diffusion coefficient of the system and H is the thickness of the fibers.

2.6. Blood Compatibility

Blood compatibility of the heparin-loaded PCL-α-TCP fibrous membranes was evaluated according to hemolytic and kinetic clotting assays. For both tests, healthy human blood from volunteer contained sodium citrate (Merck company) (3.8 wt%) diluted with normal saline (4:5 ratio by volume) was applied.

2.6.1. Hemolytic Test

Heparin-loaded PCL-α-TCP fibrous membranes with size of $10 \times 10 \times 0.2$ mm^3 ($n = 3$ for each group) were inserted in centrifuge tubes containing 10 mL normal saline and were incubated at 37 °C for 30 min. Subsequently, 200 µL of diluted blood was added to each tube and incubated for 60 min in incubator. After centrifuging the tubes for 5 min at 2700 rpm, the supernatants were removed and, ultimately, the absorbency of the solutions was measured with ultraviolet spectrophotometer at 540 nm and the hemolytic ratio (HR) was calculated (Equation (3))[44]

$$\%\mathrm{HR} = \left(\frac{A_{\mathrm{sample}} - A_n}{A_p - A_n}\right) \times 100 \tag{3}$$

where A_{sample}, A_p, and A_n represent the absorbance of samples, the positive control (distilled water) and the negative control (normal saline), respectively.

2.6.2. Kinetic Clotting Test

To evaluate the kinetic clotting, each heparin-loaded PCL-α-TCP fibrous membrane ($n = 3$) was put at the bottom of vials containing diluted blood and was maintained in incubator at 37 °C for various time points (5, 20, 35, 50, 90, and 130 min). After specific time points, the absorbance of the solutions, which were diluted by 50 mL distilled water, was measured using spectrophotometer at 540 nm.[45]

2.6.3. Platelet Adhesion

After mixing 9 mL of blood with 1 mL of 3.8% sodium citrate to prepare platelet-rich plasma (PRP), it was centrifuged at a rate of 1000 rpm for 10 min. Separately, the fibrous membranes were soaked in PRP for 30 min at 37 °C in incubator and the platelets in PRP were allowed to adhere and spread on the surface of membranes. After discarding PRP, glutaraldehyde solution (2.5 wt%) was added to the membranes for 2 h at 4 °C. Consequently, after removal of nonadherent platelets by washing the membrane surface using PBS, the adherent platelets were dehydrated using gradient immersion in 30%, 50%, 70%, 90%, 96%, and 100% ethanol for 10 min, consequently. These samples were later hydrated by critical point drying and sputtered with gold. Finally, attached platelets on blood contacting surface were evaluated using SEM.

2.7. Cell Culture Study

To investigate the role of fibrous membranes on the cell behavior, attachment, viability, and proliferation of cells were studied. Cell culture studies were performed using two cell types, MG63 cell line and Mesenchymal stem cells (MSCs). The MG63 cell line (passage number 12) and MSCs (passage number 3), obtained from Royan Institute of Iran, were cultured in Dulbecco's modified Eagle medium low glucose and DMEM/F12 (DMEM, Bioidea, Iran), respectively, supplemented with 10% v/v FBS (Bioidea, Iran), and 1% v/v penicillin/streptomycin (pen/strep, Bioidea, Iran) at 37 °C in a humidified atmosphere containing 5% CO_2. The culture medium was changed every 3 days. Before cell seeding, the samples were sterilized 30 min in 70% v/v ethanol following 2 h exposure to ultraviolent. Consequently, the membranes were immersed in complete media overnight prior to cell seeding. The cells detached with 0.25% trypsin/EDTA solution (Bioidea, Iran) and counted by trypan blue assay, were collected from the flask and seeded on the samples and tissue culture plate (TCP, control) ($n = 3$) with a density of 5000 cells per well.

The biocompatibility of the PCL-α-TCP fibrous membranes was studied by MG63 cell line via 3-(4,5-dimethylthiazolyl-2)-2,5-diphenyl tetrazolium bromide (MTT, Sigma-Aldrich, USA) assay. In this regard, at the specific time points of 1, 3, and 7 days, the culture medium was discarded and after washing with PBS, the samples were incubated with MTT solution (0.5 mg mL^{-1} MTT reagent in PBS) for 4 h. After formation of dark blue formazan, they were solubilized with the MTT solvent (DMSO) and were kept for 1 h at 37 °C on shaker. Subsequently, 100 µL of dissolved formazan solution of each sample was moved to 96-well plate and the optical density (OD) of each well was measured with a microplate reader (Bio Rad, Model 680 Instruments) at a wavelength of 540 nm. Furthermore, the potential of the heparin-loaded fibrous membrane

for proliferation of MSCs was investigated using MTT assay, at days 1, 5, and 10 of incubation, according to previous protocol.

To study the cell morphology and spreading on the heparin-loaded fibrous membrane, after 10 days of culture, cell-seeded membranes were fixed with 2.5% glutaraldehyde (Sigma-Aldrich, USA) for 3 h, dehydrated in graded ethanol, and dried in desiccator. The membranes were first coated with gold using a sputter coater and subsequently assessed using SEM. Moreover, to determine the cell spreading at day 10th, the proportion of area covered by cell at each mm^2 was calculated using ImageJ software (V. 1.51) ($n = 3$).

2.8. Statistical Analysis

All the data were expressed as means ± standard deviation and was analyzed by GraphPad Prism Software (V.6). Differences were considered statistically significant at $p < 0.05$.

3. Results and Discussion

3.1. Characterization of Si-Stabilized α-TCP Nanopowder

Although PCL reveales promising properties such as biocompatibility and relative proper mechanical characteristics, the low hydrophilicity and bioactivity lead to weak cellular interaction limiting its application in tissue engineering. To overcome these issues, various amounts of α-TCP nanopowder were incorporated into PCL fibrous membranes. In order to stabilize α-TCP powder at room temperature, Si was incorporated within TCP structure using a two-step process (Figure 1A). XRD pattern of Si-stabilized α-TCP calcified at 1250 °C (Figure 1B) demonstrated that resulting powder consisted of pure α-TCP with approved crystallinity. No evidence of the X-ray reflections relating to β-TCP or HA was found in the XRD pattern of powder proving the role of Si incorporation in postponing the typical allotropic transformation from α to β TCP. As previously illustrated in similar studies, the complete transformation of α-TCP to β-TCP without any additional chemical components was reported to occur at ≈780 °C.[46,47] Phase transition during cooling did not occur as a result of the incorporation of Si element to TCP structure. Hence, the α-TCP phase remained stable. Moreover, according to the TEM image of α-TCP powder (Figure 1C), α-TCP consisted of spherical particles with uniform shape and size and the average particle size of 10 ± 4 nm.

3.2. Characterization of PCL-α-TCP Fibrous Membrane

The bone membranes were engaged in the damaged sites with insufficient bone volume. In this regard, the membrane needs to mimic the structure of the fibrous component of the ECM and provide bioactivity and hemocompatibility to help bone regeneration. According to **Figure 2**A, electrospun fibrous membrane with specific properties consisting of large surface area and porous structure mimicking the fibrous structure of native ECM are advantageous for cell adhesion, proliferation, and migration. Incorporation of α-TCP nanopowder as a bioactive agent and heparin as drug could moderate the biocompatibility and hemocompatibility making the membranes useful for bone tissue regeneration (Figure 2A). Our results demonstrated that the morphology and average fiber size of the membranes were directly controlled via changing α-TCP nanopowder concentration. According to SEM images (Figure 2B), incorporation of α-TCP powder up to 2 wt% resulted in randomly oriented and bead-free fibers with open porosity and interconnected pores. While PCL membrane consisted of uniform fibers with smooth surface, roughness of the membranes enhanced with increasing α-TCP powder. It might be due to the formation of agglomerated particles which could clearly be detected on the PCL-2α membrane (yellow circles). Moreover, agglomerated α-TCP in fibers resulted in the formation of heterogonous fibers. In addition to morphology, average fiber and pore size of the membranes (Figure 2C,D) were changed depending on the α-TCP content. The average size of fibers was estimated ($n = 30$) and presented in Figure 2C. Results showed that while PCL membrane consisted of fibers with an average diameter of 554.5 ± 49 nm, incorporation of α-TCP resulted in significant changes in fiber diameter depending on the loading level. For instance, while the average fiber size significantly enhanced to 801.3 ± 112.9 nm after incorporation of 2 wt% α-TCP nanopowder (PCL-2α), it was reduced to about 434.3 ± 67.6 nm at PCL-0.5α membrane. It might be due to the role of α-TCP on the surface tension of solutions. By incorporation of 0.5 wt% α-TCP in PCL matrix (PCL-0.5α), the surface tension decreased compared to PCL resulted in smaller fiber size. This result was similarly reported in previous researches.[48,49] It might be due to the fact that when the surface tension decreased, the whipping motions of the fibers were modulated to the stretching motion due to the low electrostatic repulsive force.[50] For this reason, the low surface tension in PCL-0.5α solution resulted in high stretching motion rather than a whipping motion which diminished the fiber size of PCL-0.5α compared to other membranes. Moreover, increasing the amount of α-TCP in the mixture resulted in some molecular interactions between PCL and nanopowders, leading to enhanced surface tension and fiber diameters. The nature of interaction between PCL and α-TCP was investigated using FTIR spectroscopy (Figure 2E). FTIR spectrum of α-TCP consisted of the broad peak at 3000–3600 cm^{-1}, assigned to the stretching vibration of hydroxyl groups (OH). This peak could be detected at all nanocomposite fibrous membranes confirming the presence of α-TCP nanopowder within the matrix. Moreover, some peaks at 500–605, and 940–1120 cm^{-1} were assigned to the orthophosphate PO_4^{-3} group of α-TCP.[51] FTIR spectrum of PCL fibrous membrane consisted of the main characteristic peaks at 1726 cm^{-1} (stretching vibrations of the carboxyl (C—O)) and 1180 cm^{-1} (stretching vibrations of the ether groups (C—O—C)). In addition to the PCL characteristic peaks, the FTIR spectrum of PCL-2α fibrous membrane exhibited the characteristic bands of PCL and α-TCP nanopowders. Moreover, the formation of weak van der Waals interaction between PCL and α-TCP nanopowder was detected which is schematically presented at Figure 2A. The peak at 1724 cm^{-1} corresponding to C—O stretching showed considerable sensitivity to α-TCP concentration. The intensity of the peak decreased sharply and shifted to lower wavenumbers as the amount of α-TCP increased to 1 wt% indicating that the C—O group involved in hydrogen

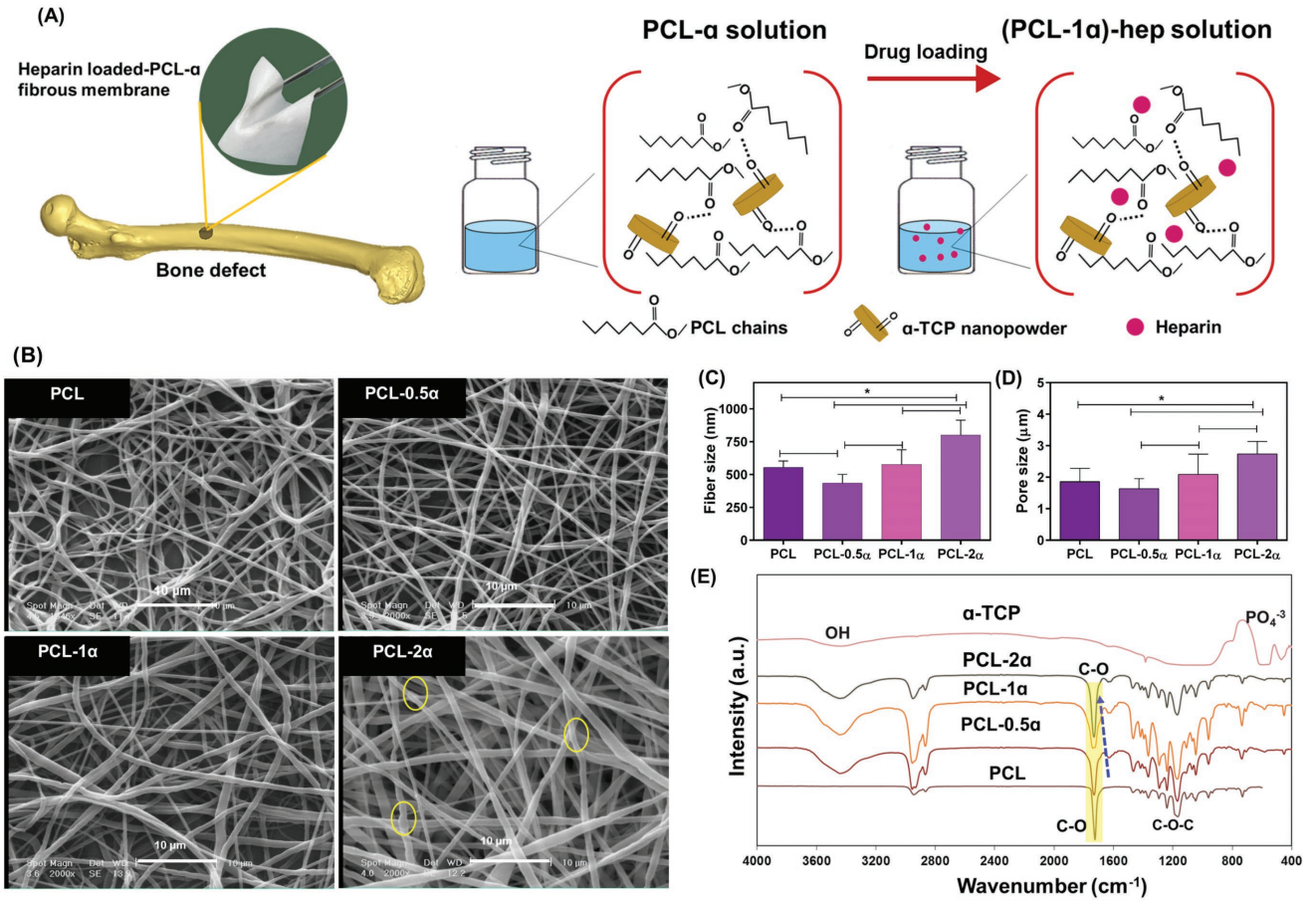

Figure 2. A) The schematic diagram of nanocomposite fibrous membrane loaded with heparin for filling bone defect. B) Structural properties of fibrous membranes evaluated by SEM images. C,D) Incorporation of α-TCP nanopowders significantly changed the average fiber and pore size of fibrous membranes (*$p < 0.05$). E) FTIR spectra of α-TCP nanopowder as well as fibrous membranes consisting of various amounts of α-TCP nanopowder.

bond formation with of α-TCP nanopowder. Afterward, by increasing the α-TCP concentration to 2 wt%, the intensity of the peak enhanced indicating that the agglomeration of α-TCP reduced the extent of interaction between PCL and α-TCP. Such these findings reported in another research focusing on the PCL-Cloisite 10A fibrous membrane developed using electrospinning technique.[52] Result demonstrated incorporation of Cloisite 10A up to 5 wt% resulted in hydrogen bonding between PCL and Cloisite 10A.

Furthermore, the porosity and surface area of fibrous membranes are of the crucial factors in designing them for tissue engineering applications. The membranes need to afford an interconnected network for uniform cell distribution during seeding and for transport of soluble signaling molecules, nutrients, and metabolic waste removal.[53] Our results revealed that the average pore size of the membranes enhanced with increasing α-TCP content (Figure 2C). This might be attributed to the increase in fiber diameter by incorporation of α-TCP into the PCL solution. For example, incorporation of α-TCP nanopowder resulted in significant increase in the average pore diameter from 1.8 ± 0.4 μm to 2.7 ± 0.4 μm at PCL-2α membrane ($P < 0.05$). The small fiber size could inhibit penetration of cells, particularly when the pore size is smaller than cells. So, the pore size of membranes need to be superior than the cell diameter.[54]

To estimate the ability of the fibrous membranes to bear the dynamic shocks and avoid rupture during surgery, they should have appropriate mechanical properties.[55,56] The appropriate range of mechanical properties for bone regeneration is estimated around 1–5 MPa tensile strength and more than 100% elongation.[55] As shown in **Figure 3**A, stress–strain curves of all membranes initially indicated a linear stress region and stretched highly with increasing strain. High porosity and the randomly oriented fibers are responsible for the low mechanical properties of electrospun membranes. However, the mechanical properties of the PCL-α-TCP fibrous membrane were significantly affected by the concentration of α-TCP nanopowders and their distribution within polymer matrices (Figure 3B–D). As demonstrated schematically in Figure 3E, incorporation of α-TCP nanopowder led to formation of some new bonds and interactions between PCL and nanopowders which enhanced the mechanical properties of the membranes. According to Figure 3B, it was found that, the tensile strength of the membranes enhanced with increasing α-TCP content up to 1 wt% α-TCP (PCL-1α). For instance, the strength of PCL fibrous membrane reached to 1.6 ± 0.5 MPa after 100% elongation. However, after incorporation of 0.5 and 1 wt% α-TCP, the tensile strength of the membranes enhanced 1.2 and 1.8 times (compared to PCL membrane), respectively. In this way, PCL-1α

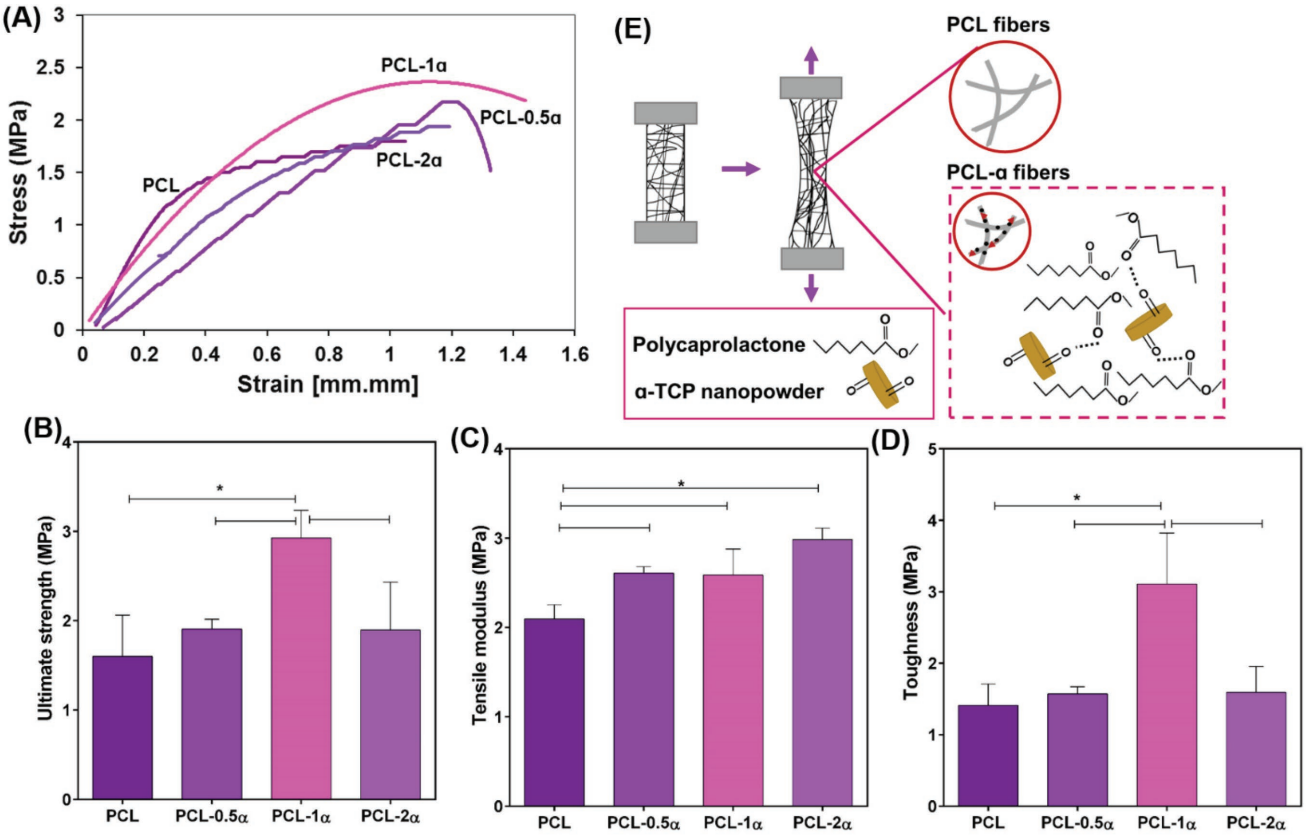

Figure 3. Mechanical properties of fibrous membranes consisting of various amounts of α-TCP nanopowders. A) Illustration of uniaxial tensile stress-strain diagram, B) the tensile strength, C) tensile modulus, and D) toughness of fibrous membranes (*$p < 0.05$). E) Schematic showing the role of nanopowder during the tensile test.

membrane revealed the robust construct with considerably higher tensile strength (2.92 ± 0.31 MPa) than PCL-0.5α (1.91 ± 0.11 MPa) and PCL (1.60 ± 0.46 MPa) fibrous membranes. Moreover, the tensile modulus of PCL-α-TCP fibrous membrane increased remarkably with respect to the neat PCL sample (Figure 3C). In particular, the tensile modulus was estimated 2.1 ± 0.2 MPa and 2.6 ± 0.3 MPa, for PCL and PCL-1α, respectively ($p < 0.05$). This indicated that α-TCP nanopowder acted as a rigid filler within the PCL matrix leading to improved strength and elastic modulus of PCL fibrous membrane. Moreover, according to Figure 3D, incorporation of α-TCP nanopowders up to 1 wt% resulted in significant improvement of toughness (2.2 times) compared to that of PCL one. However, incorporation of more α-TCP nanopowders (>1 wt%) decreased mechanical properties attributing to the aggregation of nanopowder and inhomogeneous dispersion in PCL matrix. These nanopowders acted as stress concentrators and result in lower mechanical performance.[50,57] Such these findings demonstrated in other researches.[58]

3.3. In Vitro Biological Behavior of PCL-α-TCP Fibrous Membrane

The apatite formation ability on the surface of fibrous membrane was evaluated by incubation of the membranes in SBF solution revealing the biomineralization properties of samples.[59] Owning to the hydrophobic nature and poor capability of capturing calcium ions, apatite can hardly grow on the PCL fibrous membrane, as confirmed by the SEM image (**Figure 4**A). This poor apatite formation ability of hydrophobic polymers was similarly reported for polyacrylonitrile nanofibers.[60] SEM images revealed that incorporation of α-TCP nanopowders into PCL fibers led to significant bone formation-oriented outcomes compared to that of pure PCL membrane. Cauliflower-like particles covered the surface of PCL-α-TCP membranes after soaking in SBF solution for 28 days. However, the concentration and size of cauliflower-like apatite depositions obviously enhanced when the concentration of α-TCP increased. According to EDX analysis (Figure 4B) performed on PCL-1α membrane after soaking in SBF solution, these precipitations consisted on Ca and P components with atomic ratio of 1.51 which might be related to bone-like apatite. To confirm the chemical composition of depositions on the surface of fibrous membranes, XRD analysis was also assessed on PCL-1α membrane. XRD pattern of PCL-1α after soaking for 28 days in SBF solution confirmed the presence of new peaks, along with the previous PCL characteristic peaks, ascribing to bone-like apatite.[16] According to Figure 4C, PCL showed two strong peaks located at $2\theta = 21.3°$ and 23.8°, which were respectively associated with the (110) and (200) reflections of a polyethylene-like crystal structure with orthorhombic unit cell parameters.[61]

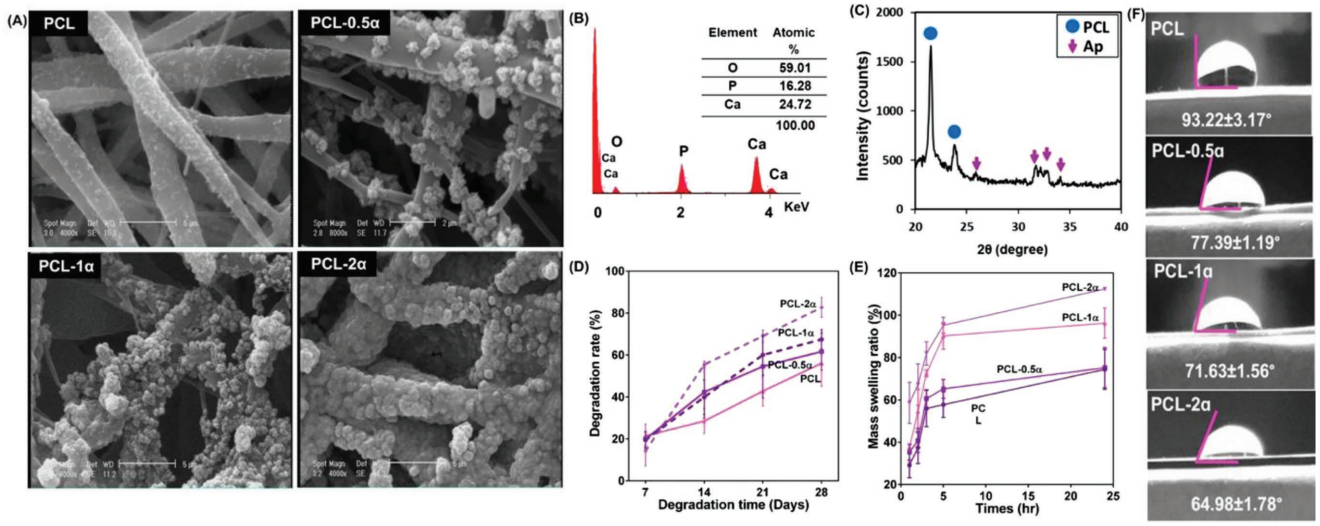

Figure 4. A) SEM images showing the surface of fibrous membranes after immersing in simulated body fluid (SBF) for 28 days. B) EDX analysis and C) XRD pattern of PCL-1α fibrous membrane after immersion in the SBF for a period of 28 days. D) The weight loss profile and E) swelling ratio of PCL-α-TCP fibrous membranes during soaking in PBS solution. F) Contact angle measurements on pristine fibrous PCL membrane and PCL-α-TCP fibrous membranes at the firs second.

Moreover, the XRD pattern of PCL-1α immersed in SBF solution indicated the Bragg peaks appearing approximately at $2\theta = 26°$, 32°, 33°, and 34°, corresponded to the characteristic reflections of (002), (211), (300), and (202) of apatite structure. However, the concentration and size of cauliflower-like apatite depositions obviously changed when the concentration of α-TCP increased. In this way, while PCL-1α membrane partially covered by a cauliflower-like apatite precipitation, the fibers of PCL-2α membrane fully covered by a layer of cauliflower-like apatite. Similarly, in a recent research, β-TCP nanopowders were incorporated in lactic acid/ PCL electrospun membrane to improve the bioactivity of scaffolds. Result showed that calcium compound deposition were observed on the composite containing 1 wt% β-TCP.[51]

The degradation properties of the membranes play a critical role in biomolecule selection in tissue engineering. According to Figure 4D, the degradation profiles of PCL-α-TCP fibrous membrane with different α-TCP concentrations were similar to that of PCL one (with a lower rate of degradation). It was clear that all PCL-α-TCP fibrous membranes continued to degrade over the entire incubation period (28 days). In addition, the weight loss percentage of PCL-α-TCP fibrous membrane varied with different concentrations of α-TCP nanopowder. At lower concentrations of α-TCP (0.5 and 1 wt%), after 28 days of incubation, the weight loss was only about 61.7 ± 8% and 67.5 ± 4%, respectively, which was not significantly different compared to that of PCL fibrous membrane (56.1 ± 11%) ($P > 0.05$). Between all samples, PCL-α-TCP membrane consisting of 2% α-TCP revealed the highest weight loss owning to the aggregating of α-TCP nanopowders, the weak interaction between PCL chains and nanopowders as well as high hydrophilicity of samples. This behavior was similarly reported for PCL-multiwall carbon nanotube (MWCNT) fibrous scaffolds in which MWCNT addition accelerated the weight loss behavior compared to pristine PCL.[62] The results of swelling ratio (Figure 4E) and water contact angle measurements (Figure 4F) confirmed the weight loss results. Swelling ratio results demonstrated that incorporation of α-TCP nanopowder resulted in rapid swelling of the membranes within the initial 5 h, and maintained almost a steady increase until the end of the test (24 h). Noticeably, the swelling ratio of PCL membrane after 24 h immersing was 74.4 ± 9.5% which increased significantly ($P < 0.05$) to 112.4 ± 0.2% when 2 wt% α-TCP nanopowder was incorporated within the PCL fibers. Similarly, incorporation of TCP nanopowder remarkably enhanced the hydrophilicity of fibrous PCL-TCP scaffolds.[63,64]

Moreover, the water contact angle measurements were also determined to the hydrophilicity of the membranes (Figure 4D). Our results revealed the water contact angle of the PCL fibrous membrane reduced by incorporation of α-TCP to PCL matrices. For example, the water contact angle of fibrous PCL membrane was 93.2° ± 3.2° which significantly reduced to 64.9° ± 1.8° for PCL-2α fibrous membrane. Similar results were described for PCL-20 wt% β-TCP in which water contact angle reduced from 110° (for pure PCL scaffold) to 78°.[64]

In order to evaluate the role of α-TCP nanopowder on the cell responses, the proliferation of MG63 osteoblast-like cells seeded on the PCL-α-TCP fibrous membrane was evaluated after 1, 3, and 7 days of culture using an MTT assay (**Figure 5**). Results revealed that MG63 cells proliferated well with passing time. However, cell proliferation on PCL-α-TCP fibrous membranes was significantly higher than that of PCL after 7 days ($p < 0.05$), indicating the role of α-TCP nanopowder on the biological properties of PCL fibrous membrane. For example, the viability of cells on the PCL-1α and PCL-2α reached to 166.3 ± 12.4 (% control) and 196.0 ± 17.0 (% control), respectively, while the cell viability on PCL fibrous membrane was 74.8 ± 7.9 (% control) after 7 days of culture ($p < 0.05$). It might be due to the hydrophilicity of the fibrous membrane which enhanced by incorporation of α-TCP nanopowder (Figure 4D). Similar result was demonstrated in other researches in which the cells could adhere to the hydrophilic substrates significantly

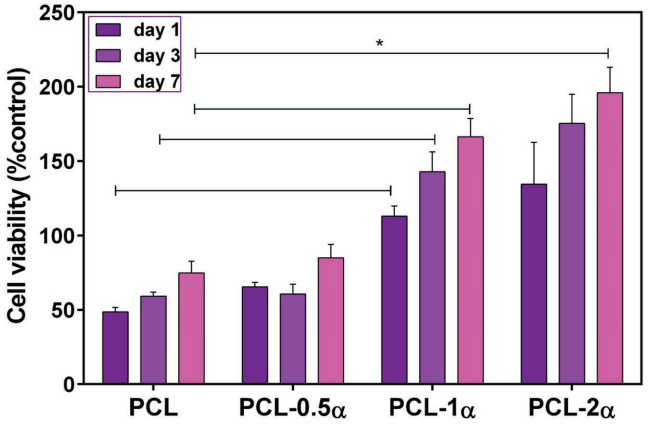

Figure 5. The viability of MG63 cells cultured on various fibrous membranes for 1, 3, and 7 days ($n = 3$) (*$p < 0.05$).

compared to hydrophobic one.[61,65] Moreover, according to SEM images, the presence of α-TCP significantly increased the cell proliferation due to enhanced protein absorption ability of the fibrous membrane due to the presence of α-TCP and also rougher surface due to the presence of α-TCP aggregations on fiber surface providing the extra sites for cell binding (Figure 1A). Introducing α-TCP nanopowders into the PCL fibrous matrix not only provided mechanical support, but also improved the biocompatibility of PCL, which would also advantageous for osteoblast proliferation. The similar results reported in another research focused on the β-TCP-poly(lactic acid) fibrous membrane.[66] According to the characteristics of PCL-α-TCP fibrous membrane, the PCL-1α membrane revealed the promising mechanical, physical and biological properties making it an appropriate membrane for further hemocompatibility evaluation.

3.4. Characterization of Heparin-Loaded PCL-α-TCP Fibrous Membranes

The surface morphology of heparin-loaded PCL-α-TCP fibrous membranes was evaluated using SEM analysis. As demonstrated in **Figure 6**A, the morphology of different heparin-loaded membranes was homogenous and bead free. However, the fiber diameter was changed significantly with increasing amounts of heparin content ($p < 0.05$). According to Figure 6B, the addition of heparin resulted in reduce in the fiber size from 554.5 ± 48.8 nm (for PCL-1α) to 317.4 ± 117.7 nm (for (PCL-1α)-2hep). Such similar results demonstrated in another research[67] and might be due to role of heparin content on the modulation of viscosity and electrical conductivity of solution.[68,69] Thanks to the ionic nature of heparin, the ionic strength and the conductivity of the electrospun solutions enhanced leading to larger elongation force and consequently decrease in average fiber diameter of membranes.

The chemical properties of heparin-loaded fibers were analyzed by FTIR spectroscopy (Figure 6C). Heparin consisted of the characteristic absorption peaks at about 1090 and 1237 cm^{-1} assigned to the symmetric and asymmetric stretching vibrating of O=S=O group, respectively. Moreover, the C—O stretch of COOH in the heparin molecule was assigned at 1237 cm^{-1}. Finally, the band at 1054 cm^{-1} was attributed to the SO_3 group of heparin.[70] Furthermore, the characteristic peaks of PCL-1α at 500–605 and 940–1120 cm^{-1} were assigned to the orthophosphate groups of α-TCP. In addition the main characteristic peaks of PCL at 1726 cm^{-1} assigned to C—O groups, and 1180 cm^{-1} for C—O—C were identified in FTIR spectrum. The existence of these characteristic bands implied that heparin incorporated in PCL-α-TCP fibers without any destruction in its structure.

Heparin release profiles from fibrous membrane PCL-1α with different heparin proportions (0.5, 1, and 2 wt%) are presented in Figure 6D. Experiments were performed in triplicate and the amount of α-TCP release was determined. Results revealed that, electrospun fibrous membranes exhibited fast heparin release (50–60%) during the initial stage (6 days) followed by a relatively constant release. The fast release of heparin might be effective to prevent myeloproliferative response as heparin treatment begun immediately at the time of injury is more effective than a delayed administration.[71] In this way, after 14 days of incubation, the total amounts of released heparin from (PCL-1α)-0.5hep, (PCL-1α)-1hep and (PCL-1α)-2hep membranes were 70.3 ± 2.1%, 74.8 ± 3.3%, and 77.2 ± 1.6%, respectively. It was consistent with the release profiles attained by another research group.[71] It indicated that smaller fibers of membranes (Figure 6A) resulted in shorter paths for diffusion of drug molecules and, difference in the rate of swelling and relaxation of the respective membrane which changed the penetration and diffusion of PBS through the membranes and, consequently, the rate of drug release.

To analyze the mechanism of heparin release, the fractional amount of heparin released was plotted against the square root of time and the release exponent (n), rate parameter (k), and apparent diffusion coefficient (D_{app}) of the systems were calculated (Figure 6E and **Table 1**). According to Figure 6E, the Fickian diffusional release of the heparin from the fibrous membranes was s uggested. Moreover, according to the correlation coefficients of the regressions (R^2) (Table 1), it was found that this equation was acceptable to describe the mechanism of heparin release from the presented membranes. Moreover, according to Table 1, the release rate of heparin from the fibrous membranes was not significantly different for the three heparin-loaded membranes. According to Table 1, the release exponent was 0.5 or less for the membranes which revealed that the system was diffusion-controlled. So, the exponent of heparin release from the membrane was 0.166, 0.169, and 0.182 for (PCL-1α)-0.1hep, (PCL-1α)-1hep, and (PCL-1α)-2hep, respectively, which did not show any significant difference.

3.5. In Vitro Biological Behavior of Heparin-Loaded PCL-α-TCP Fibrous Membrane

3.5.1. Hemocompatibility Evaluation

One of the main critical issues interfering the application of the membranes for bone graft substitutes, is their potency of

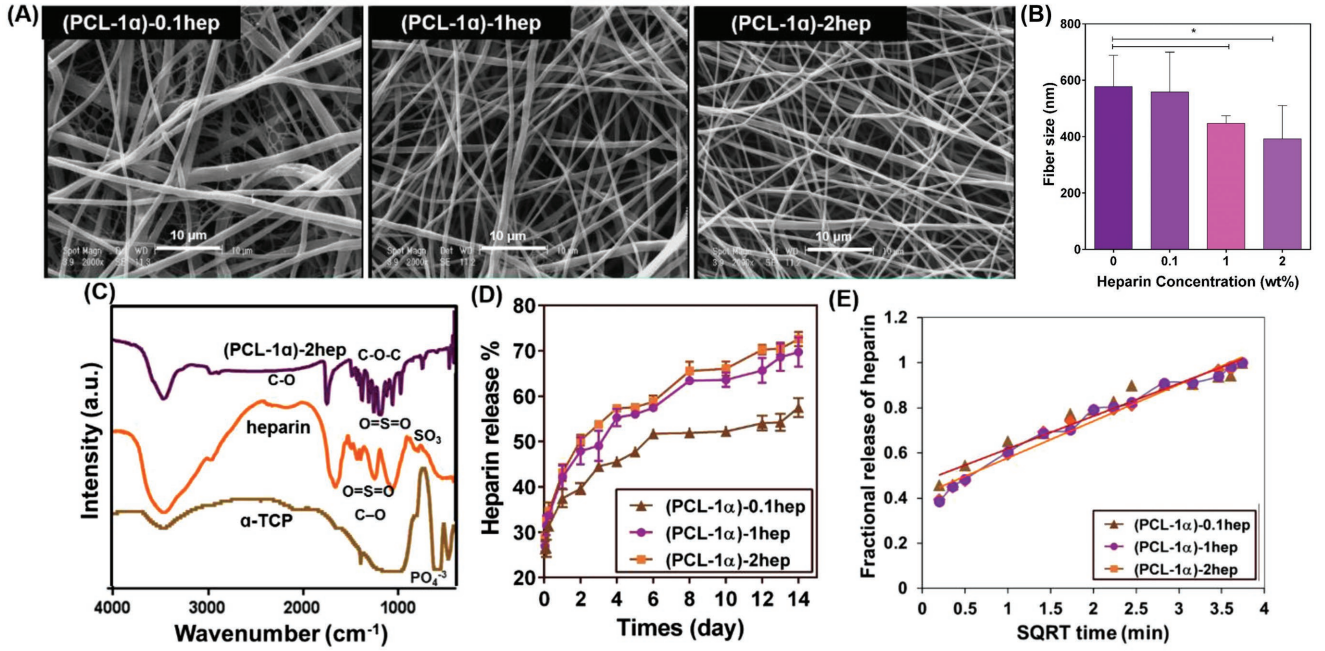

Figure 6. A) SEM images of various heparin-loaded PCL-1α fibrous membranes. B) Fiber size distribution on the heparin-loaded PCL-1α fibrous membranes as a function of heparin content (*: $P < 0.05$). C) FT-IR spectra of α-TCP powder, heparin, and (PCL-1α)-2hep fibrous membrane. D) Cumulative release of heparin from PCL-1α fibrous membranes consisting of 0.1, 1, and 2 wt% heparin into PBS at 37 °C. E) Fractional release of heparin from PCL-1α fibrous membranes consisting of various amounts of heparin plotted as a function of the square root of time.

hemolysis in contact with blood.[72] The interaction results in the damage of blood cellular membrane or the erythrocytes lysis leading to the release of their intracellular hemoglobin. The amount of released hemoglobin should be small to ensure the absence of toxicity of the implanted material.[40] Moreover, hemocompatibility of membranes in contact with bone tissue could affect osseointegration.[73] In this regard, heparin can interact with a great number of proteins relating to adhesion (e.g., fibronectin and vitronectin), proliferation (e.g., fibroblast growth factor), or osteogenic differentiation (e.g., bone morphogenic proteins).[33]

The hemocompatibility of heparin-loaded PCL-α-TCP membranes was investigated via the percentage of hemolysis, kinetic clotting, and platelet adhesion assays. **Figure 7**A shows the percentage of hemolysis obtained after the direct contact between blood and the membranes. Results revealed that the hemolysis degree decreased as the amount of the heparin increased. While the hemolysis degrees of PCL-1α was 6.6 ± 0.2%, it was reduced to 4.9 ± 0.3%, 3.5 ± 0.4%, and 2.6 ± 0.1% on the (PCL-1α)-0.1hep, (PCL-1α)-1hep, and (PCL-1α)-2hep membranes, respectively. This behavior might be due to the molecular basis for the anticoagulant action of heparin thanks to its capability to bind to and improve the inhibitory activity of the plasma protein anti-thrombin against numerous serine proteases of the coagulation system, most importantly factors IIa (thrombin), Xa and IXa.[74] Moreover, the pore size of the membranes is crucial for the hemolysis evaluation. Results demonstrated that the pore size more than 6.2–8.2 μm could lead to ability of erythrocytes to penetrate into the membranes.[75] Incorporation of heparin within PCL-1α membrane resulted in reduced pore size to 1.49 μm which could not facilitate the interaction of erythrocytes with the whole surface of the membranes. Recently, the blood interactions with two inert bioinspired ceramic scaffolds obtained from natural resources (biomorphic carbon and silicon carbides (bioSiC) from different origins) were studied. They showed that there is a critical pore size above which the erythrocytes (mean size 7.5 μm) are able to penetrate into the biomorphic carbon and silicon carbides scaffolds with the pore size of 141 μm.[75]

When a foreign material is exposed to blood, plasma proteins adsorbed followed by the activation of clotting factors or the adhesion and activation of platelets, and finally the formation of non-soluble fibrin network or thrombus.[76] Therefore, the aim of in vitro dynamic clotting time test was to measure the activation extent of coagulation factor and the clotting time influenced by the material. The longer clotting time results in better anticoagulation of the material. In this research, heparin used as a blood anticoagulant could catalytically promote formation rate of antithrombin III (AT III) and inhibit thrombin (TB) and some other coagulating proteases. According to Figure 7B, it could be determined that the blood incubated with (PCL-1α)-2hep membranes had significantly

Table 1. The drug release parameters of the heparin-loaded fibrous membranes.

Sample	Model parameters			$D_{app} \times 10^{+19}$ [$m^2\ s^{-1}$]
	n	K [$s^{-0.5}$]	R^2	
(PCL-1α)-0.1hep	0.166	0.056231	0.949	2.15
(PCL-1α)-1hep	0.169	0.28064	0.973	3.16
(PCL-1α)-2hep	0.182	0.056721	0.974	3.42

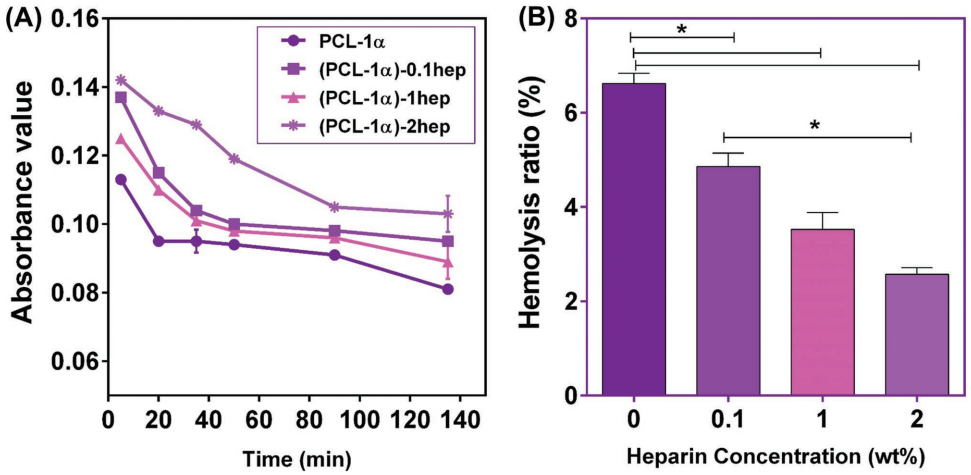

Figure 7. Effect of heparin release from PCL-1α fibrous membranes on the blood interaction: A) Kinetic clotting curves plotted as a function of time and heparin content. B) Hemolysis ratio as function of heparin loaded (*$p < 0.05$).

higher absorbance than PCL-1α at each time point. Moreover, after 20 min exposure of PCL-1α membrane to the human red blood cells, blood coagulated, while no obvious hemolytic phenomenon could be detected, even after 50 min of exposure to other membranes. In addition, there was no significant difference in the degree of clotting until 50 min with the increasing concentration of heparin content. These results showed that (PCL-1α)-2hep membranes revealed good anticoagulant and hemocompatibility property. Such these results demonstrated in other research in which the effect of surface modification of chitosan/heparin polyelectrolyte complex was evaluated. Their results showed that heparinized PAN membranes could reduce the thrombus formation.[76]

The blood compatibility of the PCL-1α and (PCL-1α)-hep fibrous membrane was also studied by platelet adhesion tests of PRP. Platelet spreading and aggregation on the surfaces are marks of platelet activation, which is considered to be a major mechanism of thrombosis. According to **Figure 8**, incorporation of heparin within the membrane is an effective method to avoid thrombus formation and to improve the hemocompatibility of blood-contacting biomaterials. SEM images showed that red blood cells (RBCs) and activated platelets (indicated by red arrows) adhesion were in a high degree on PCL-1α and (PCL-1α)-0.1hep and led to the formation of a fibrin network on the fibrous membrane. According to previous researches, the size of platelets and red blood cells are different. While the size

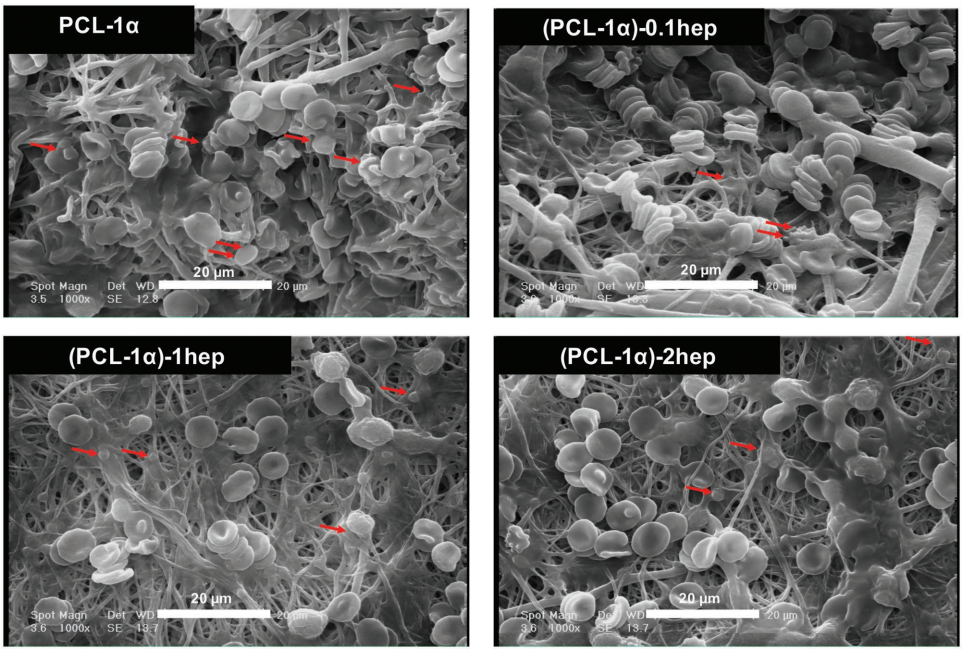

Figure 8. SEM images of adherent platelets on PCL-1α fibrous membranes consisting of various concentrations of heparin (red arrows showed platelets).

of platelets is in the range of 2–4 μm, the RBC size is in the range of 8–10 μm,[77,78] making them detectable in the images. However, the incorporation of more heparin as a hemocompatible drug led to less attachments and spreading of platelets for (PCL-1α)-1hep and (PCL-1α)-2hep. These findings represented in other research which platelets were visible on the PCL scaffolds.[31,79]

3.5.2. Biocompatibility Evaluation of (PCL-1α)-hep Fibrous Membranes

Heparin is a bioactive material which helps immobilize the growth factors, and thus improves cell viability in vitro. However, the negative charges of heparin molecules have been suggested to inhibit cell proliferation.[80] Therefore, the aim of this study was to evaluate the right concentration of heparin which can promote MCS proliferation. As can be seen in **Figure 9**A, heparin-loaded fibrous membranes showed relatively higher cell viability during the culture period than PCL-1α one ($*p < 0.05$). After the first day of culture, release of heparin from the fibrous membranes resulted in significantly enhanced (1.6 times) cell viability from 71.3 ± 3.8 (% control) (for PCL-1α) to 109.6 ± 8.2 (% control)) (for (PCL-1α)-1hep) ($*p < 0.05$). It might be due to the interaction of heparin with proteins and absorption of higher amounts of proteins compared to unmodified membrane. Our results revealed that the cell viability on (PCL-1α)-hep did not show a significant change compared to the PCL-1α after 5 days of culture. Furthermore, the data revealed an increase in cell viability and proliferation when MSCs were cultured on the membranes containing 0.1 and 1 wt% heparin after 10 days compared to the non-heparinized membrane ($*p < 0.05$). Noticeably, the viability of MSCs on the PCL-1α membrane (192.1 ± 28.3 (%control)) enhanced 1.4 and 1.2 times compared to on (PCL-1α)-0.1hep and (PCL-1α)-1hep, respectively ($*p < 0.05$).

Although release of heparin was maintained during the culture period, (PCL-1α)-2hep did not induce the cell proliferation related to extra amount of heparin releasing during 10 days. As revealed in heparin release studies (Figure 6D), more than 60% of the immobilized heparin released from (PCL-1α)-2hep fibrous membrane during the first 10 days of culture. Similar results was demonstrated in other research which by adding heparin more than 0.25 mg, the cell viability decreased remarkably.[80] This result was due to the fact that the high contents of L-Iduronic acid (IdoA) and *N*-sulphonylated GlcN which are essential components in heparin molecules, correlated to its ability to inhibit cell proliferation.[81] So, it is important to choose a proper concentration of heparin which help to proliferate cells.

After 10 days of MSC culture, the cell-fibrous membrane constructs were visualized by SEM to evaluate the cell morphology (Figure 9B). MSCs cultured on the fibrous membranes revealed an elongated shape and adhered to the pores, suggesting strong cell adhesion and biocompatibility. Moreover, according to the estimated average cell area after 10 days of culture (Figure 9C), MSCs covered more surface area of the (PCL-1α)-1hep membrane than that of PCL-1α (2.57 times) ($P < 0.05$). It might be due to the fact that heparin could interact with the proteins in serum which have important roles in cellular attachment onto surfaces. So, (PCL-1α)-hep membranes adsorb higher amounts of these proteins compared to PCL-1α membrane. Similar findings were demonstrated in other research. It was proved the simulative effect of covalently bound heparin on the proliferation of MC3T3-E1 preosteoblasts cells.[33]

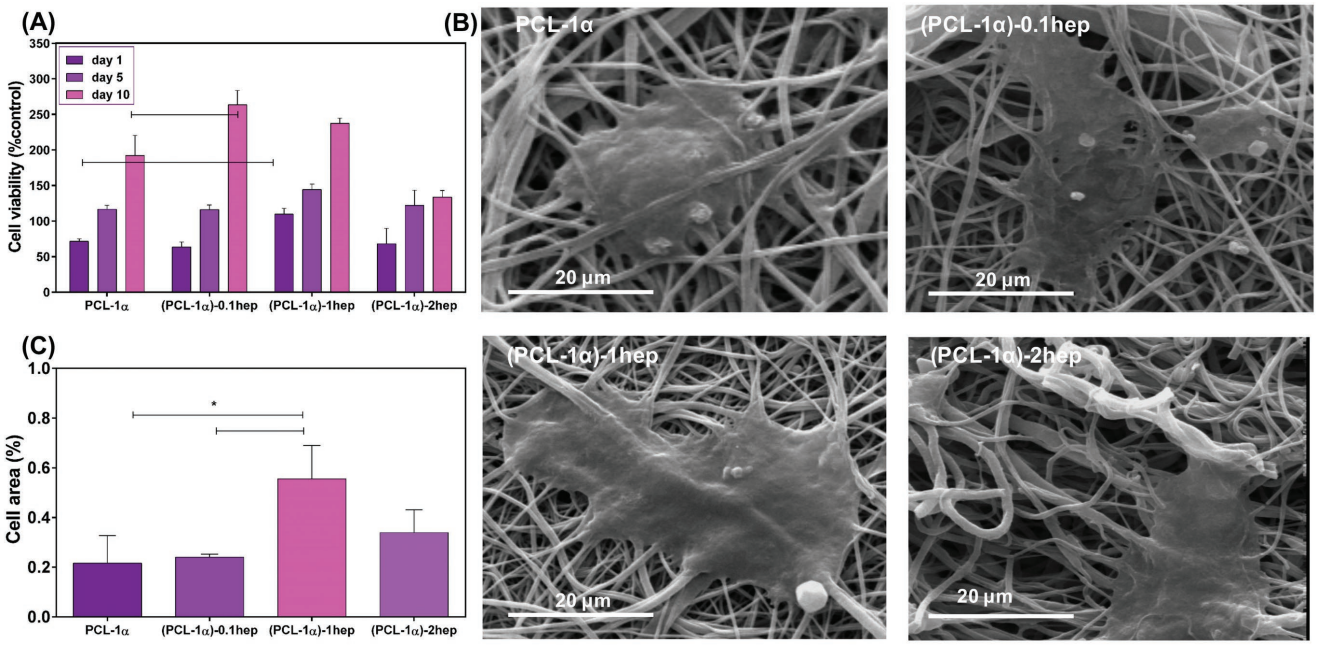

Figure 9. A) Evaluation of cell viability by MTT assay after 10 days of MSC culture on various heparin-loaded PCL-1α fibrous membranes ($n = 3$) ($*p < 0.05$). B) SEM images of MSCs on different heparin-loaded PCL-1α fibrous membranes at the 10th days of MSC culture on the PCL-1α membrane. C) The fraction of surface area of fibrous membranes covered with MSCs, as a function of heparin content ($*P < 0.05$).

4. Conclusions

In this research, PCL-based fibrous nanocomposite membranes embedded with spherical α-TCP nanopowders were engineered as a drug carrier to use as hemocompatible and bioactive substrates for bone tissue engineering. The focus of the work was to shed light on the differences in chemical, mechanical, and hemocompatibility of the membranes which had α-TCP nanopowder and heparin as drug. Results showed that the incorporation of 1 wt% α-TCP nanopowder (PCL-1α membrane) resulted in enhanced mechanical properties (1.8 times greater in strength), bioactivity, and hydrophilicity of the PCL-based membranes. Therefore, at low concentrations of α-TCP nanopowders, the membrane could be an appropriate candidate for regenerative bone tissue. Moreover, the addition of heparin to PCL-1α fibrous membrane not only modulated hemocompatibility but also improved proliferation and attachment of MSC. Results indicated that incorporation of heparin decreased the hemolysis ratio of the PCL-1α fibrous membrane. Moreover, the number of platelet adhesion decreased significantly with increasing heparin content. Our results suggested that heparin-loaded PCL-α-TCP membrane could be an ideal membrane for bone tissue applications at the optimal concentration of α-TCP nanopowder and heparin (1 wt%) which will give proper mechanical, structural, and hemocompatibility properties.

Conflict of Interest

The authors declare no conflict of interest.

Keywords

bone tissue engineering., fibrous membrane, hemocompatibility, heparin, α-tricalcium phosphate

Received: January 15, 2018
Revised: March 21, 2018
Published online:

[1] C. Perka, O. Schultz, R.-S. Spitzer, K. Lindenhayn, G.-R. Burmester, M. Sittinger, *Biomaterials* **2000**, *21*, 1145.
[2] S. N. Parikh, *Orthopedics* **2002**, *25*, 1301.
[3] M. Mehta, K. Schmidt-Bleek, G. N. Duda, D. J. Mooney, *Adv. Drug Delivery Rev.* **2012**, *64*, 1257.
[4] M. Roozbahani, M. Alehosseini, M. Kharaziha, R. Emadi, *Mater. Sci. Eng. C* **2017**, *81*, 532.
[5] M. Diba, M. Fathi, M. Kharaziha, *Mater. Lett.* **2011**, *65*, 1931.
[6] M. Kharaziha, M. H. Fathi, H. Edris, N. Nourbakhsh, A. Talebi, S. Salmanizadeh, *J. Mater. Sci.: Mater. Med.* **2015**, *26*, 36.
[7] M. Kharaziha, M. Fathi, H. Edris, *Compos. Sci. Technol.* **2013**, *87*, 182.
[8] M. Diba, F. Tapia, A. R. Boccaccini, L. A. Strobel, *Int. J. Appl. Glass Sci.* **2012**, *3*, 221.
[9] Y. Dai, Y. Xia, H.-B. Chen, N. Li, G. Chen, F.-M. Zhang, N. Gu, *J. Bioact. Compat. Polym.* **2016**, *31*, 152.
[10] H. Su, K. Y. Liu, A. Karydis, D. G. Abebe, C. Wu, K. M. Anderson, N. Ghadri, P. Adatrow, T. Fujiwara, J. D. Bumgardner, *Biomed. Mater.* **2016**, *12*, 015003.
[11] K. Tuzlakoglu, R. L. Reis, *Tissue Eng., Part B* **2008**, *15*, 17.
[12] S. D. McCullen, Y. Zhu, S. H. Bernacki, R. J. Narayan, B. Pourdeyhimi, R. E. Gorga, E. G. Loboa, *Biomed. Mater.* **2009**, *4*, 035002.
[13] J. H. Shim, J. B. Huh, J. Y. Park, Y. C. Jeon, S. S. Kang, J. Y. Kim, J. W. Rhie, D. W. Cho, *Tissue Eng., Part A* **2013**, *19*, 317.
[14] M. S. Kim, G. H. Kim, *Mater. Lett.* **2014**, *120*, 246.
[15] L.-n. Jia, X. Zhang, H.-y. Xu, F. Hua, X.-g. Hu, Q. Xie, W. Wang, J. Jia, *J. Nanomater.* **2016**, *2016*, 1.
[16] F. Yang, S. K. Both, X. Yang, X. F. Walboomers, J. A. Jansen, *Acta Biomater.* **2009**, *5*, 3295.
[17] M. Kikuchi, Y. Koyama, T. Yamada, Y. Imamura, T. Okada, N. Shirahama, K. Akita, K. Takakuda, J. Tanaka, *Biomaterials* **2004**, *25*, 5979.
[18] A. A. Ignatius, M. Ohnmacht, L. E. Claes, J. Kreidler, F. Palm, *J. Biomed. Mater. Res.* **2001**, *58*, 564.
[19] Y. Hosseini, R. Emadi, M. Kharaziha, A. Doostmohammadi, *J. Appl. Polym. Sci.* **2017**, *134*, 44433.
[20] H. W. Kim, J. C. Knowles, H. E. Kim, *J. Biomedical Mater. Res., Part A* **2004**, *70*, 467.
[21] X. Zhang, S. Meng, Y. Huang, M. Xu, Y. He, H. Lin, J. Han, Y. Chai, Y. Wei, X. Deng, *Stem Cells Int.* **2015**, *2015*, 507154.
[22] H. Yuan, J. De Bruijn, Y. Li, J. Feng, Z. Yang, K. De Groot, X. Zhang, *J. Mater. Sci. Mater. Med.* **2001**, *12*, 7.
[23] J. Kolmas, A. Kaflak, A. Zima, A. Slosarczyk, *Ceram. Int.* **2015**, *41*, 5727.
[24] L. Yubao, Z. Xingdong, K. de Groot, *Biomaterials* **1997**, *18*, 737.
[25] R. Vani, E. K. Girija, K. Elayaraja, S. Prakash Parthiban, R. Kesavamoorthy, S. Narayana Kalkura, *J. Mater. Sci. Mater. Med.* **2009**, *20 Suppl 1*, S43.
[26] M. Kitamura, C. Ohtsuki, S.-i. Ogata, M. Kamitakahara, M. Tanihara, *Mater. Trans* **2004**, *45*, 983.
[27] V. Linda, G. Karlis Agris, R. Una, Y. Thomas Chung-Kuang, *Biomed. Mater.* **2015**, *10*, 025009.
[28] L. M. Ehrenfried, M. H. Patel, R. E. Cameron, *J. Mater. Sci.: Mater. Med.* **2008**, *19*, 459.
[29] S. M. Bennett, M. Arumugam, S. Wilberforce, D. Enea, N. Rushton, X. C. Zhang, S. M. Best, R. E. Cameron, R. A. Brooks, *Acta Biomater.* **2016**, *45*, 340.
[30] M. Fini, G. Giavaresi, N. N. Aldini, P. Torricelli, R. Botter, D. Beruto, R. Giardino, *Biomaterials* **2002**, *23*, 4523.
[31] H. Jiang, X. B. Wang, C. Y. Li, J. S. Li, F. J. Xu, C. Mao, W. T. Yang, J. Shen, *Langmuir* **2011**, *27*, 11575.
[32] J. Lee, J. Yoo, A. Atala, S. Lee, *Acta Biomater.* **2012**, *8*, 2549.
[33] M. Gumusderelioglu, S. Aday, *Carbohydr. Res.* **2011**, *346*, 606.
[34] E. Luong-Van, L. Grøndahl, K. N. Chua, K. W. Leong, V. Nurcombe, S. M. Cool, *Biomaterials* **2006**, *27*, 2042.
[35] J. Lee, J. J. Yoo, A. Atala, S. J. Lee, *Acta Biomater.* **2012**, *8*, 2549.
[36] Z. X. Meng, W. Zheng, L. Li, Y. F. Zheng, *Mater. Sci. Eng., C* **2010**, *30*, 1014.
[37] S. Wang, Y. Zhang, H. Wang, Z. Dong, *Int. J. Biol. Macromol.* **2011**, *48*, 345.
[38] Y. Shibata, Y. Abiko, K. Goto, Y. Moriya, H. Takiguchi, *Biochem. Int.* **1992**, *28*, 335.
[39] J.-H. Jiang, L.-P. Zhu, X.-L. Li, Y.-Y. Xu, B.-K. Zhu, *J. Membr. Sci.* **2010**, *364*, 194.
[40] C. Cao, Y. Song, Q. Yao, Y. Yao, T. Wang, B. Huang, P. Gong, *J. Biomater. Sci., Polym. Ed.* **2015**, *26*, 600.
[41] I. Martinez, P. Velásquez, L. Meseguer-Olmo, A. Bernabeu-Esclapez, P. De Aza, *Mater. Sci. Eng., C* **2012**, *32*, 878.
[42] M. Yashima, A. Sakai, *Chem. Phys. Lett.* **2003**, *372*, 779.
[43] N. Golafshan, R. Rezahasani, M. T. Esfahani, M. Kharaziha, S. Khorasani, *Carbohydr. Polym.* **2017**.
[44] Y.-H. Zou, R.-C. Zeng, Q.-Z. Wang, L.-J. Liu, Q.-Q. Xu, C. Wang, Z.-W. Liu, *Front. Mater. Sci.* **2016**, *10*, 281.

[45] B. P. Zhang, H. Qiu, D. W. Wang, Y. Q. Liu, Z. G. Bi, *J. Biomed. Mater. Res., Part A* **2011**, *99*, 166.
[46] E. R. Kreidler, F. A. Hummel, *Inorg. Chem.* **1967**, *6*, 884.
[47] I. R. Gibson, I. Rehman, S. M. Best, W. Bonfield, *J. Mater. Sci. Mater. Med.* **2000**, *11*, 799.
[48] M. Kharaziha, S. R. Shin, M. Nikkhah, S. N. Topkaya, N. Masoumi, N. Annabi, M. R. Dokmeci, A. Khademhosseini, *Biomaterials* **2014**, *35*, 7346.
[49] M. Kharaziha, M. H. Fathi, H. Edris, *Compos. Sc. Technol.* **2013**, *87*, 182.
[50] N. Golafshan, M. Kharaziha, M. Fathi, *Carbon* **2016**.
[51] C.-H. Park, E. K. Kim, L. D. Tijing, A. Amarjargal, H. R. Pant, C. S. Kim, H. K. Shon, *Ceram. Int.* **2014**, *40*, 5049.
[52] P. Vashisth, K. Nikhil, P. Roy, P. A. Pruthi, R. P. Singh, V. Pruthi, *Carbohydr. Polym.* **2016**, *136*, 851.
[53] L. Ghasemi-Mobarakeh, M. P. Prabhakaran, M. Morshed, M. H. Nasr-Esfahani, S. Ramakrishna, *Tissue Eng., Part A* **2009**, *15*, 3605.
[54] K. Sisson, C. Zhang, M. C. Farach-Carson, D. B. Chase, J. F. Rabolt, *J. Biomed. Mater. Res., Part A* **2010**, *94*, 1312.
[55] A. K. Gaharwar, S. Mukundan, E. Karaca, A. Dolatshahi-Pirouz, A. Patel, K. Rangarajan, S. M. Mihaila, G. Iviglia, H. Zhang, A. Khademhosseini, *Tissue Eng., Part A* **2014**, *20*, 2088.
[56] K. Fujihara, M. Kotaki, S. Ramakrishna, *Biomaterials* **2005**, *26*, 4139.
[57] N. Golafshan, M. Kharaziha, M. Fathi, B. L. Larson, G. Giatsidis, N. Masoumi, *RSC Adv.* **2018**, *8*, 6381.
[58] A. Bianco, E. Di Federico, I. Cacciotti, *Polym. Adv. Technol.* **2011**, *22*, 1832.
[59] Y. Hosseini, R. Emadi, M. Kharaziha, *Mater. Chem. Phys.* **2017**, *194*, 356.
[60] J. Wang, W. Qin, X. Liu, H. Liu, *RSC Adv.* **2013**, *3*, 11132.
[61] M. G. Yeo, G. H. Kim, *Chem. Mater.* **2012**, *24*, 903.
[62] Z. Meng, W. Zheng, L. Li, Y. Zheng, *Mater. Sci. Eng., C* **2010**, *30*, 1014.
[63] Y. Zhou, D. W. Hutmacher, S. L. Varawan, T. M. Lim, *Polym. Int.* **2007**, *56*, 333.
[64] M. Yeo, H. Lee, G. Kim, *Biomacromolecules* **2010**, *12*, 502.
[65] M. Yeo, W.-K. Jung, G. Kim, *J. Mater. Chem.* **2012**, *22*, 3568.
[66] T. Lou, X. Wang, G. Song, Z. Gu, Z. Yang, *Int. J. Biol. Macromol.* **2014**, *69*, 464.
[67] J.-O. Jeong, S. I. Jeong, J.-S. Park, H.-J. Gwon, S.-J. Ahn, H. Shin, J. Y. Lee, Y.-M. Lim, *RSC Adv.* **2017**, *7*, 8963.
[68] J. Zeng, H. Haoqing, A. Schaper, J. H. Wendorff, A. Greiner, *e-Polymers* **2003**, *3*, 102.
[69] C. Santos, C. J. Silva, Z. Büttel, R. Guimarães, S. B. Pereira, P. Tamagnini, A. Zille, *Carbohydr. Polym.* **2014**, *99*, 584.
[70] M. M. Sk, C. Y. Yue, R. K. Jena, *RSC Adv.* **2014**, *4*, 5188.
[71] E. Luong-Van, L. Grondahl, K. N. Chua, K. W. Leong, V. Nurcombe, S. M. Cool, *Biomaterials* **2006**, *27*, 2042.
[72] Y. Zhao, S. Wang, Q. Guo, M. Shen, X. Shi, *J. Appl. Polym. Sci.* **2013**, *127*, 4825.
[73] I. Denry, L. T. Kuhn, *Dent. Mater.* **2016**, *32*, 43.
[74] R. Lever, B. Mulloy, C. P. Page, *Heparin - A Century of Progress*, Springer Science & Business Media **2012**.
[75] P. Diaz-Rodriguez, P. Gonzalez, J. Serra, M. Landin, *Mater. Sci. Eng., C* **2014**, *41*, 232.
[76] W.-C. Lin, T.-Y. Liu, M.-C. Yang, *Biomaterials* **2004**, *25*, 1947.
[77] I. Pleines, A. Eckly, M. Elvers, I. Hagedorn, S. Eliautou, M. Bender, X. Wu, F. Lanza, C. Gachet, C. Brakebusch, *Blood* **2010**, *115*, 3364.
[78] A. A. Hanke, S. Maschler, H. Schöchl, F. Flöricke, K. Görlinger, K. Zanger, P. Kienbaum, *Scand. J. Trauma, Resus. Emerg. Med.* **2011**, *19*, 12.
[79] M. Rampichová, M. Buzgo, A. Míčková, K. Vocetková, V. Sovková, V. Lukášová, E. Filová, F. Rustichelli, E. Amler, *Int. J. Nanomed.* **2017**, *12*, 347.
[80] F. Aleahmad, T. Talaei-Khozani, S. Rajabi-Zeleti, M. Sani, S. Jalili-Firoozinezhad, S. Bonakdar, S. Heshmat-Azad, M. Azarnia, M. Jaberipour, *Hepatitis Mon.* **2017**, *17*, e40599.
[81] D. Nikitovic, A. Zafiropoulos, G. Tzanakakis, N. Karamanos, A. Tsatsakis, *Anticancer Res.* **2005**, *25*, 2851.